

Mossbauer and Magnetic Studies of Lithium Zinc Ferrites and Lithium Manganese Ferrites

Dr.N.Vasudevan Nair(Rtd)^{a*}, S.Resmi^b

^aDepartment of Physics, MG College, Thiruvananthapuram- 695004, Kerala

^bHSST, SSVGHSS, Chirayinkeezhu, Thiruvananthapuram-695304, Kerala

Abstract: This paper presents the studies on Mossbauer and magnetization properties of Lithium Zinc Ferrites (LZF) and Lithium Manganese Ferrites (LMF). Mossbauer spectroscopy provides powerful probe to the chemical and the magnetic state of all atoms. Lithium based ferrites are potential magnetic material for micro wave applications. They possess a spinel (AB₂O₄) type crystal structure. For LZF, Isomer shift for A site (IS_A) is less than that for B site (IS_B) for all samples. The quadruple splitting for A site (dQ_A) is greater than the quadruple splitting for B site (dQ_B) except for the composition $x=0.2$. The hyperfine magnetic field for B site (H_B) varies in between 514 KOe and 428 KOe and the hyperfine magnetic field for A site (H_A) varies in between 479 KOe and 327 KOe. For LMF Isomer shift for A site (IS_A) is less than that for B site (IS_B) for all samples.. The quadrupole splitting for A-site varies in between 0.001 to 0.4263 and for B-site it varies in between 0.0276 to 0.3763 mm/s. The hyperfine field for B site (H_B) varies in between 510 KOe and 517 KOe and that for A site (H_A) varies in between 449 KOe and 481 KOe. The magnetization for Zn samples reaches the saturation value below field of 1.5 KOe and that for Mn samples is below a field of 2 KOe. For LZF there is also evidence that the magnetic order for large X involves micro magnetic tendencies as well as canting, and for LMF net magnetization increases and reaches maximum value for $x=0.2$ sample. Curie temperature decreases linearly for LZF samples and non linearly for LMF samples with increase of concentration. Permeability increases with increase in temperature for LZF and linear increase of permeability with temperature for LMF.

Keywords: Lithium Zinc and Lithium Manganese Ferrites, Mossbauer spectroscopy, Magnetization, Curie temperature, Permeability.

Date of Submission: 07-04-2019

Date of acceptance: 23-04-2019

I. Introduction

Ferrites are considered to be the best magnetic materials for high and very high frequency circuits. Lithium based ferrite, as it promises to be a potential magnetic material for applications such as circulators, phase shifters, isolators, memory core, antennas, power transformation in electronics, high speed digital tapes etc. Spinel ferrite particle is an ideal small particle magnetic system as the crystal chemistry issue can be controlled. The magnetic properties of spinel ferrites arise from the ability of the compound to distribute the metal ions among the available A and B sites. Non magnetic substitutions in ferrites alter the inter and intra sub lattice exchange interaction between the magnetic ions. This gives rise to a variety of magnetic properties in ferrites.

This topic present the studies on the Mossbauer and magnetization properties of the Lithium Zinc Ferrites(LZF) and Lithium Manganese Ferrites(LMF).

1.2 Mossbauer studies

Mossbauer spectroscopy provides excellent tool to understand the chemical state and the environment of all atoms. With the advent of nanoscience, the scope of this branch increased. It gives unique information and also complements result obtained using other techniques such as X-ray diffraction and magnetization measurement. Information about the cation distribution can be obtained from the areas, magnetic field and line width of spectra.

1.3 Experimental Details

The Mossbauer spectrum of LZF series and LMF series were taken with a Mossbauer spectrometer in the constant acceleration mode in transmission geometry. All the samples were examined in the powder form. 20 mg of powder is sandwiched between two cello tapes covering an area of about one square cm. The quantity of active material kept low to minimize the broadening of the spectral lines. A natural iron foil has used as the

standard absorber for calibration. The data was collected for about 24 hours to ensure good absorption peaks and the experiment was performed at room temperature 300k. The absorber was kept stationary and the source was kept moving. The maximum velocity was limited to about 10 mm/s. The gamma rays were detected by argon-methane proportional counter. Data analysis was done on folded spectra containing 256 channels. All the spectra were taken without an applied magnetic field. The Mossbauer spectrum is fitted to Lorentzian lines by the method of least squares. Using the calibration spectra of standard iron, the velocity per channel is calculated.

1.4 Result and Discussion

1.4.1 $\text{Li}_{0.5}\text{Fe}_{2.5}\text{O}_4$

The Mossbauerspectra of lithium ferrite is shown in Fig (1.1). The dots in the figures represent the experimental data and the continuous lines of the least square fitting. This pattern can be attributed the distribution of iron at tetrahedral (A) and octahedral (B) sites. It gives the ferrimagnetic behaviour of the sample.

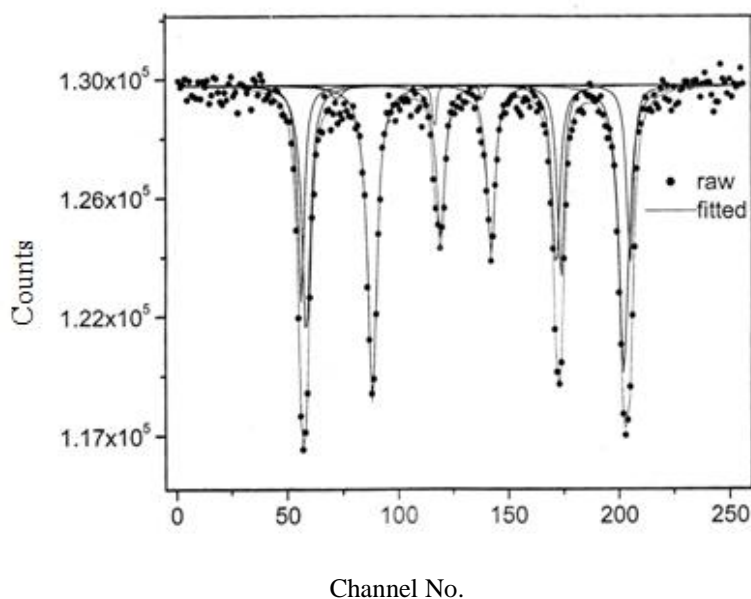


Fig. (1.1) Mossbauer spectra of $\text{Li}_{0.5}\text{Fe}_{2.5}\text{O}_4$

The Mossbauer parameters such as isomer shifts quadrupole splitting, and hyper fine magnetic field for A and B sub spectra are given in table 1.1. The isomer shift is found positive. The value of isomer shift indicate that the iron ions at both sites are ferric.

Isomer Shift for A site (IS_A) is 0.2421 mm/s and Isomer Shift for B Site (IS_B) is 0.3077 mm/s. The quadrupole splitting corresponds to B site (dQ_B) is 0.077 mm/s and that of A site (dQ_A) is 0.241 mm/s dQ_A is greater than dQ_B .

The B-site has a hyperfine field (H_B) 514 KOe which is greater than metallic iron. (H_A) is 479 KOe. $H_B > H_A$. The hyper fine field at octahedral B sites of inverse spinel is found to be near 550KOe, when the B-site iron Ion has only Fe^{3+} neighbours at A site.

Table (1.1) Mossbauer parameters of Lithium Zinc Ferrites at 300K

Sample	Is. Shift (mm/s)		Q.S (mm/s)		Hyperfine field (kOe)	
	A	B	A	B	A	B
$\text{Li}_{0.5}\text{Fe}_{2.5}\text{O}_4$ (x=0)	0.2421	0.3077	0.241	0.0773	479	514
$\text{Li}_{0.4}\text{Zn}_{0.2}\text{Fe}_{2.4}\text{O}_4$ (x=0.2)	0.3003	0.3109	0.062	0.1385	455	495
$\text{Li}_{0.35}\text{Zn}_{0.3}\text{Fe}_{2.35}\text{O}_4$ (x=0.3)	0.2707	0.2925	0.3788	0.0952	425	491
$\text{Li}_{0.3}\text{Zn}_{0.4}\text{Fe}_{2.3}\text{O}_4$ (x=0.4)	0.1617	0.2571	0.3463	0.1754	395	479
$\text{Li}_{0.25}\text{Zn}_{0.5}\text{Fe}_{2.25}\text{O}_4$ (x=0.4)	0.2572	0.2618	0.4298	0.2193	345	430
$\text{Li}_{0.2}\text{Zn}_{0.6}\text{Fe}_{2.2}\text{O}_4$ (x=0.5)	0.2329	0.3841	1.152	0.1511	327	428

1.4.2 Lithium Zinc Ferrites

The Mossbauer spectra of LZF series shown 1.2.a to 1.2.e. The Mossbauer spectra exhibit two super imposed asymmetric Zeeman sextets due to A-site and B-site Fe^{3+} ions.

The Mossbauer parameters are shown in the table 1.1. The value of the isomer shift relative to the natural iron for all samples varies between 0.1617 mm/s and 0.3003 mm/s, for A sites and 0.2571 mm/s to 0.3841 mm/s for B sites. IS_A is less than IS_B for all samples. Isomer shift of A site is lesser than B site can be due to large bond separation in $\text{Fe}^{3+} - \text{O}^{2-}$ for octahedral compared to that of tetrahedral ions. $\text{IS}_A < \text{IS}_B$, shows that iron is in the Fe^{+3} state.

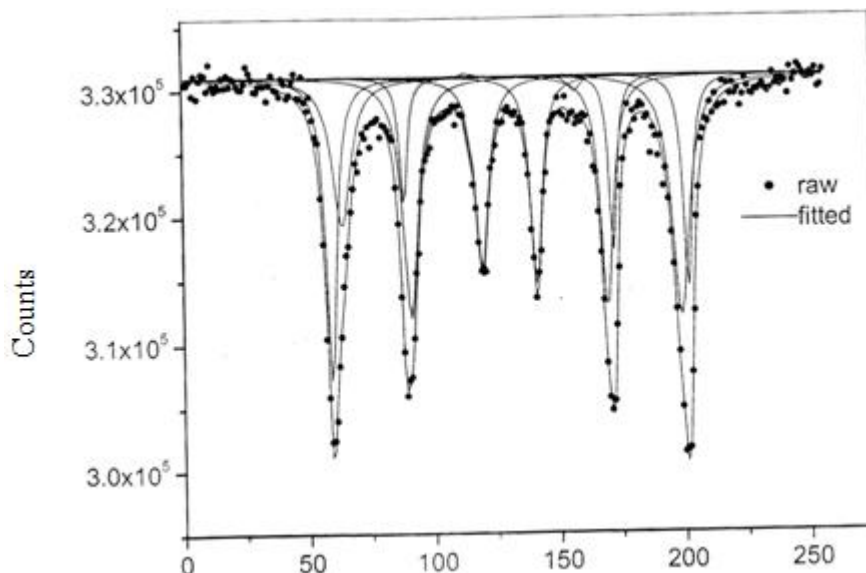


Fig. 1.2.a Mossbauer spectra of $\text{Li}_{0.4}\text{Zn}_{0.2}\text{Fe}_{2.4}\text{O}_4$

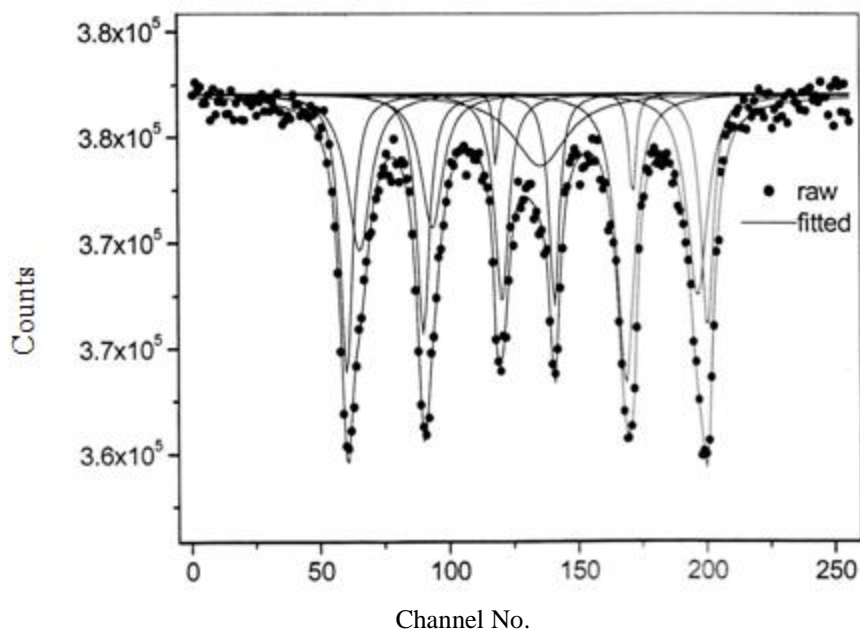


Fig. 1.2.b Mossbauer spectra of $\text{Li}_{0.35}\text{Zn}_{0.3}\text{Fe}_{2.35}\text{O}_4$

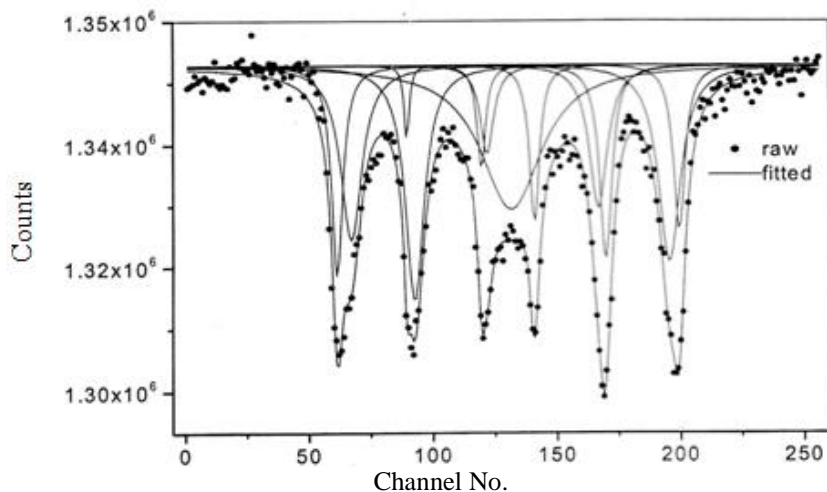


Fig. 1.2.c Mossbauer spectra of $\text{Li}_{0.3}\text{Zn}_{0.4}\text{Fe}_{2.3}\text{O}_4$

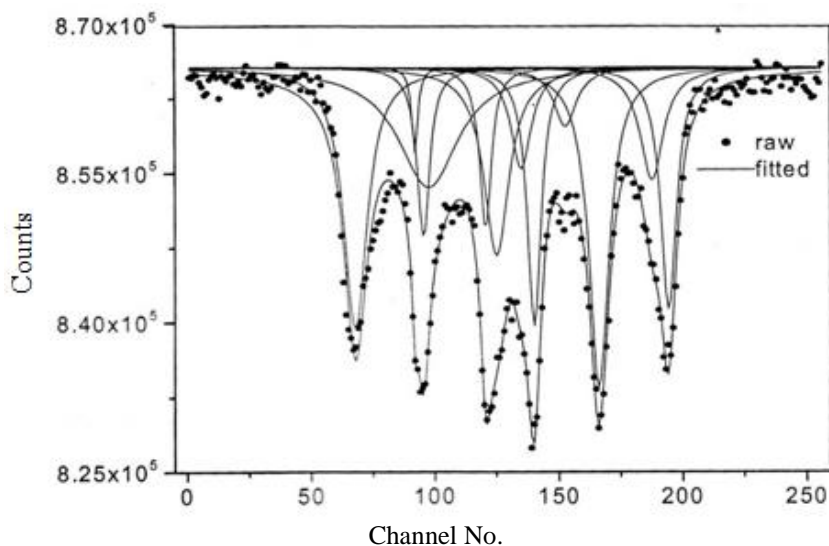


Fig. 1.2.d Mossbauer spectra of $\text{Li}_{0.25}\text{Zn}_{0.5}\text{Fe}_{2.25}\text{O}_4$

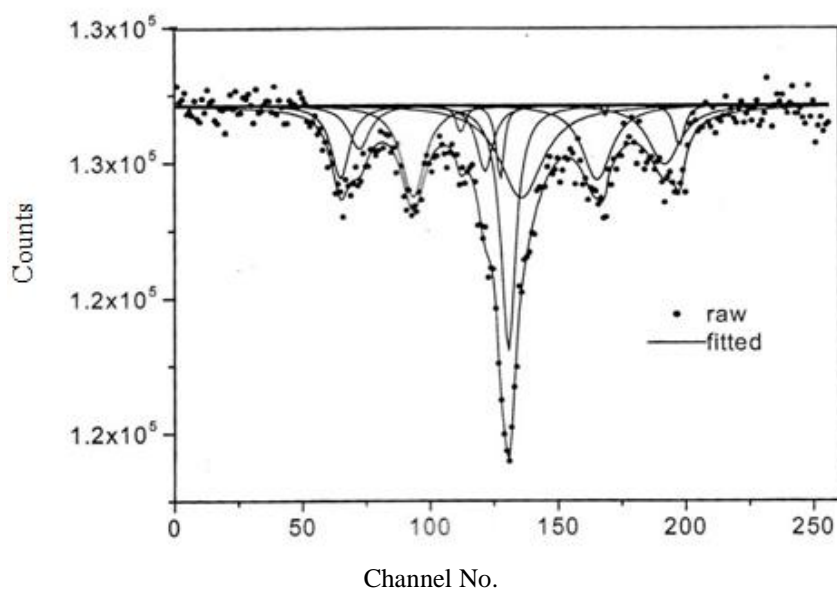


Fig. 1.2.e Mossbauer spectra of $\text{Li}_{0.2}\text{Zn}_{0.6}\text{Fe}_{2.2}\text{O}_4$

For all samples A-site isomer-shift are found to about 0.1mm/sec more negative than those for the B-site. The isomer shift obtained from the present study vary as a function of zinc concentration.

The quadrupole splitting corresponds dQ_B varies between 0.0773 and 0.2193 mm/s and dQ_A varies between 0.062 and 1.152mm/s. dQ_A is greater than dQ_B except for the composition $X=0.2$.

The hyper fine field H_B varies in between 514 kOe and 428 kOe for B-site and H_A varies in between 479 kOe and 327kOe for A site. The nuclear hyperfine field for A-site is lower than that of B-site. The variation of hyperfine field at A and B sites as a function of Zn concentration are shown in Fig 1.3(a) and 1.3(b).

The hyper fine magnetic field at the A and B sites decreases with the increase in substitution of Zn^{2+} . This decrease in hyperfine field reflects the difference in the super exchange interaction $Zn(A)-O-Fe(B)$ and $Fe(A)-O-Fe(B)$.

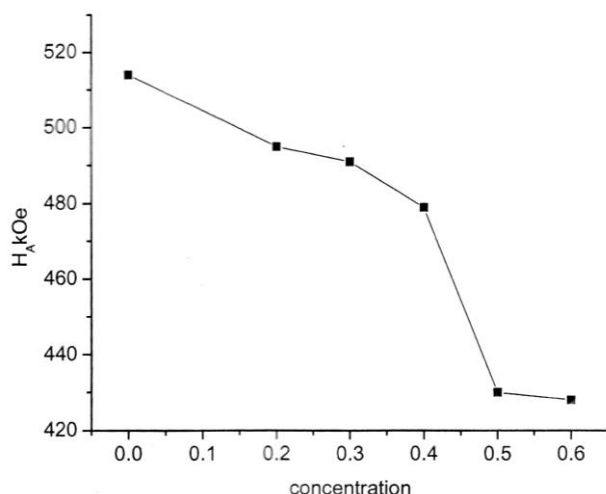


Fig. 1.3.a. Hyperfine field at B site as a function of Zn concentration

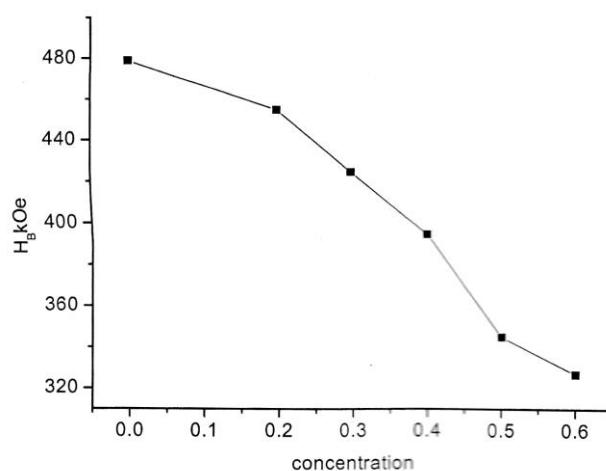


Fig. 1.3.b. Hyperfine field at A site as a function of Zn concentration

Mossbauer effect has revealed the presence of multiple hyperfine field at Fe^{3+} nuclei in B-sites. As the 2 and 5 lines are not disappeared in the spectra for all the samples, we can obtain information in the spin arrangement. That is there exists a non collinear spin configuration which is helical spin structure. The existence of canted spin structure can be obtained from the Mossbauer spectra of Lithium Zinc ferrites. The spectra having composition $x \geq 0.4$ experience relaxation behaviour in both A and B sites. The relaxation behaviour is found to increase with increases of x .

The well defined spectra in the case of $x = 0$ to 0.5 is to not seen in the case of $x = 0.6$. The six line spectrum was blurred and a broad single line is observed at the centre. This is due to super paramagnetism.

The spectrum of the sample with $x = 0.6$ shows super paramagnetic behaviour. A number of properties of zinc substituted ferrites including the saturation magnetization have been explained by Gilleo as being due to the presence of super paramagnetic clusters with the material.

1.4.3 Lithium Manganese Ferrites

The Mossbauer spectra of LMF shown from 1.4(a) to 1.4(e). The dots represent the continuous lines of the least square fitting. Well defined Zeeman patterns consisting of six separate sextets were observed for all samples. These patterns can be attributed to the distribution of iron at tetrahedral (A) and octahedral (B) sites. It indicates the ferrimagnetic behaviour of sample.

Table 1.2 Mossbauer parameters of Lithium Manganese ferrite at 300 K

Sample	Is. Shift (mm/s)		Q.S (mm/s)		Hyperfine field (kOe)	
	A	B	A	B	A	B
Li _{0.5} Fe _{2.5} O ₄ (x=0)	0.2421	0.3077	0.241	0.0773	479	514
Li _{0.4} Zn _{0.2} Fe _{2.4} O ₄ (x=0.2)	0.3389	0.3403	0.001	0.0276	466	517
Li _{0.35} Zn _{0.3} Fe _{2.35} O ₄ (x=0.3)	0.2977	0.3056	0.1867	0.12	478	511
Li _{0.3} Zn _{0.4} Fe _{2.3} O ₄ (x=0.4)	0.2195	0.3146	0.4263	0.1515	472	510
Li _{0.25} Zn _{0.5} Fe _{2.25} O ₄ (x=0.5)	0.3203	0.4029	0.0135	0.1523	449	516
Li _{0.2} Zn _{0.6} Fe _{2.2} O ₄ (x=0.6)	0.2860	0.3505	0.1099	0.3765	481	511

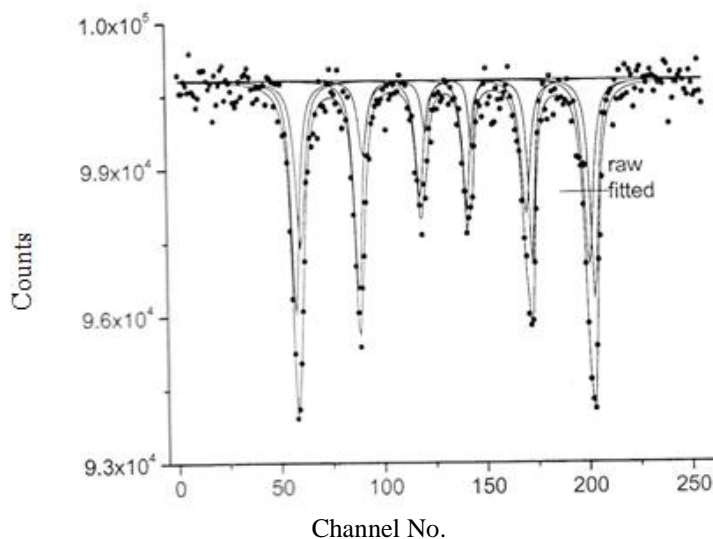


Fig. 1.4.a Mossbauer spectra of Li_{0.4}Mn_{0.2}Fe_{2.4}O₄

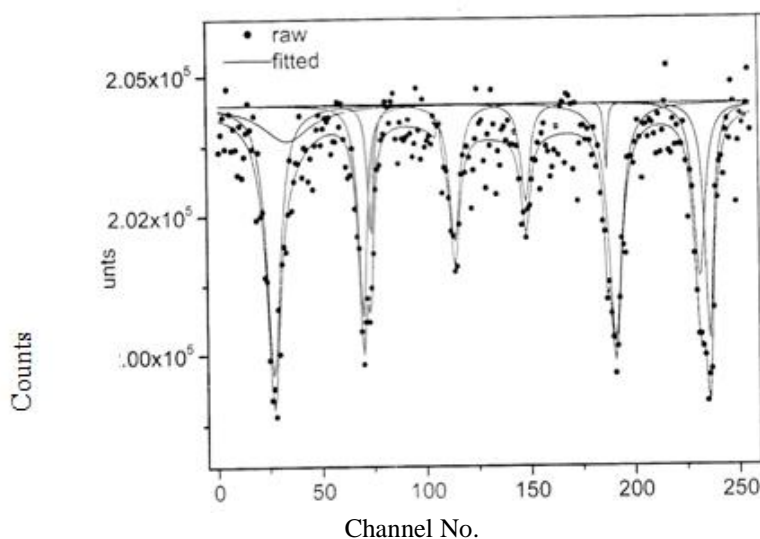


Fig. 1.4.b Mossbauer spectra of Li_{0.4}Mn_{0.2}Fe_{2.4}O₄

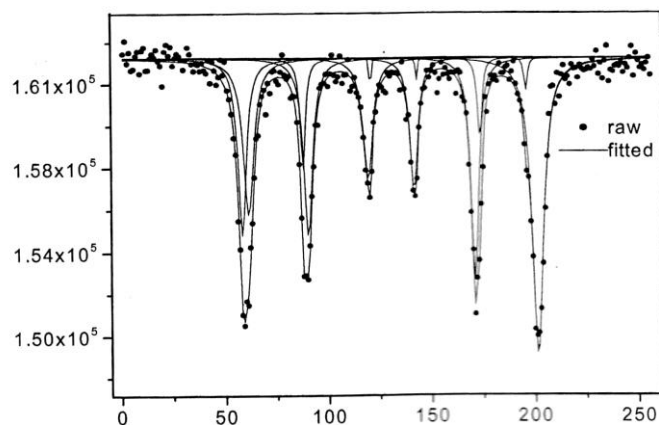


Fig. 5.4.c. Mossbauer spectra of $\text{Li}_{0.3}\text{Mn}_{0.4}\text{Fe}_{2.3}\text{O}_4$

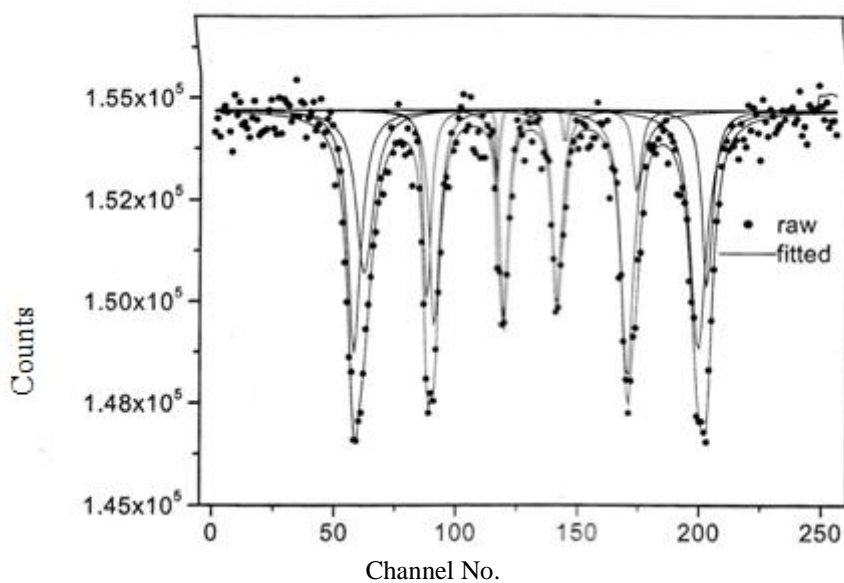


Fig. 5.4.d. Mossbauer spectra of $\text{Li}_{0.25}\text{Mn}_{0.5}\text{Fe}_{2.25}\text{O}_4$

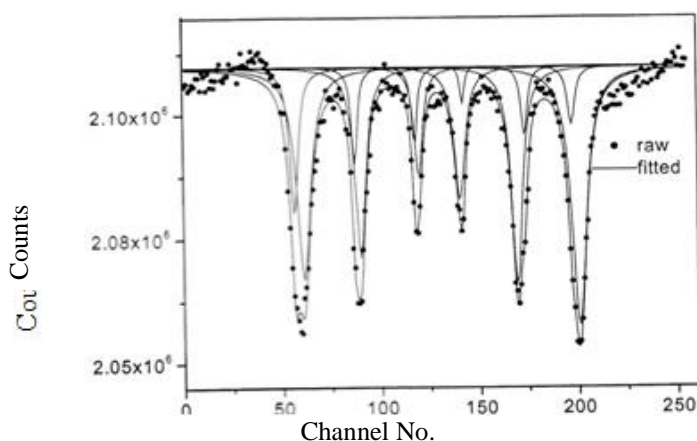


Fig. 5.4.e. Mossbauer spectra of $\text{Li}_{0.2}\text{Mn}_{0.6}\text{Fe}_{2.2}\text{O}_4$

IS_A varies in between 0.2195 mm/s and 0.3389 mm/s and IS_B varies between 0.3056 mm/s and 0.4209 mm/s. This indicates the substitution of Mn influences the s-electron charge density of ferrite. $IS_A < IS_B$ for all samples.

The quadrupole splitting for A sites varies in between 0.001 to 0.4263 and for B sites it varies in between 0.0276 to 0.3765 mm/s. From $x = 0.2$, quadruple splitting increases for B-site due to higher electric field asymmetry. H_B varies in between 510 kOe and 517 KOe and H_A varies in between 449 KOe and 481 KOe. Variation of hyper fine field with Mn concentration is as shown in Fig. 1.5.

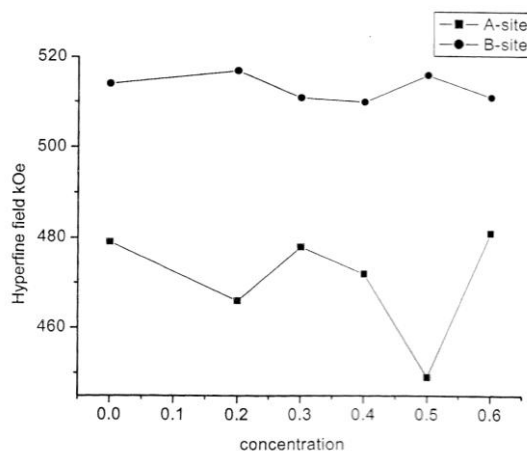


Fig.1.5 Hyperfine field at A & B site as a function of Mn

1.4.4 Recoilless fraction and Debye Temperature

These two are estimated using the following equations.

Recoilless fraction of the absorber

$$f_a = \frac{T_a}{P_s + t_e}$$

T_a is the total effective absorption thickness $t_e = 0.578 \text{ cm}^2/\text{mg}$ for Fe^{57}

The Debye temperature calculated using the equation.

$$f = \frac{-6E_R T}{K_B \theta_D^2}$$

E_R is the recoil energy, θ_D is the Debye temperature, K_B is Boltzmann constant

Table (1.3) Recoilless fraction and Debye Temperature of Lithium Zinc Ferrites

Sample	Recoilless fraction (f_a)		Debye Temperature (K)	
	A	B	A	B
$\text{Li}_{0.5}\text{Fe}_{2.5}\text{O}_4$ ($x=0$)	0.101	0.191	134	158
$\text{Li}_{0.4}\text{Zn}_{0.2}\text{Fe}_{2.4}\text{O}_4$ ($x=0.2$)	0.295	0.215	184	164
$\text{Li}_{0.35}\text{Zn}_{0.3}\text{Fe}_{2.35}\text{O}_4$ ($x=0.3$)	0.288	0.182	182	156
$\text{Li}_{0.3}\text{Zn}_{0.4}\text{Fe}_{2.3}\text{O}_4$ ($x=0.4$)	0.247	0.087	172	130
$\text{Li}_{0.25}\text{Zn}_{0.5}\text{Fe}_{2.25}\text{O}_4$ ($x=0.5$)	0.541	0.219	259	165
$\text{Li}_{0.2}\text{Zn}_{0.6}\text{Fe}_{2.2}\text{O}_4$ ($x=0.6$)	0.276	0.207	179	162

Table (1.4) Recoilless fraction and Debye Temperature of Lithium Manganese Ferrites

Sample	Recoilless fraction (f_a)		Debye Temperature (K)	
	A	B	A	B
$\text{Li}_{0.5}\text{Fe}_{2.5}\text{O}_4$ ($x=0$)	0.101	0.191	134	158
$\text{Li}_{0.4}\text{Zn}_{0.2}\text{Fe}_{2.4}\text{O}_4$ ($x=0.2$)	0.139	0.188	145	157
$\text{Li}_{0.35}\text{Zn}_{0.3}\text{Fe}_{2.35}\text{O}_4$ ($x=0.3$)	0.021	0.109	103	136
$\text{Li}_{0.3}\text{Zn}_{0.4}\text{Fe}_{2.3}\text{O}_4$ ($x=0.4$)	0.153	0.328	148	192
$\text{Li}_{0.25}\text{Zn}_{0.5}\text{Fe}_{2.25}\text{O}_4$ ($x=0.5$)	0.159	0.448	150	227

$\text{Li}_{0.2}\text{Zn}_{0.6}\text{Fe}_{2.2}\text{O}_4$ ($x=0.6$)	0.128	0.093	142	132
--	-------	-------	-----	-----

The recoilless fraction varies in between 0.101 and 0.541 for A site, 0.087 and 0.219 for B site for LZF samples. The Debye temperature varies from 134K to 259K for A site and 130K and 165K for B site. The maximum value of Debye temperature is obtained for the sample $x = 0.5$ for LZF.

For LMF samples the recoilless fraction varies in between 0.021 and 0.159 for A site, 0.093 and 0.448 for B site. The Debye temperature varies from 103k to 150k for A site and 132k and 227k for B site. The maximum value of Debye temperature is obtained for the sample $x = 0.5$ of LMF.

1.5 Magnetization Measurements

1.5.1 Experimental Details

A PAR model 155 vibrating sample magnetometer was used for the study of magnetization of the material. A nickel sample was used as a standard to calibrate measured magnetic moment, the electromagnet capable of producing a field up to 12kG. A sample of (.05 gm) taken in a glass ampoule of 1mm ID and placed in the VSM. The magnetic moment measured at room temperature from 500 G to about 2KG.

1.5.2 Result and Discussion

Fig. 1.6 shows the magnetic moment of Lithium Zinc Ferrite sample plotted as a function of field at room temperature. Also Fig. 1.7 shows the magnetic moment of LMF samples plotted as a function of field at room temperature. Below a field of 1.5 kOe Zn samples reaches the saturation values and below the field of 2kOe Mn samples reaches the saturation value.

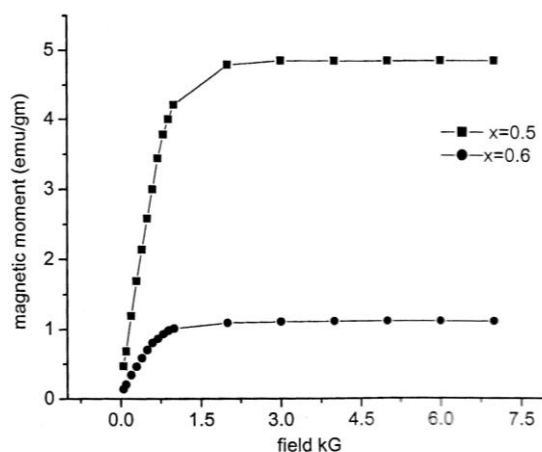


Fig.1.6 Magnetization Vs applied field for $\text{Li}_{0.5-x/2}\text{Zn}_x\text{Fe}_{2.5-x/2}\text{O}_4$ ($x=0.5,0.6$)

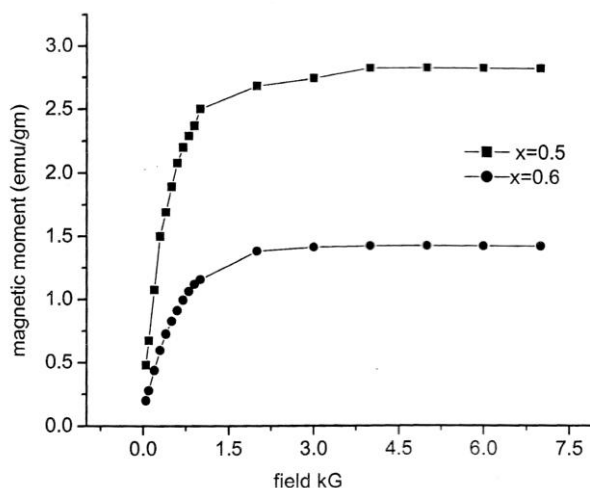


Fig.1.7 Magnetization Vs applied field for $\text{Li}_{0.5-x/2}\text{Mn}_x\text{Fe}_{2.5-x/2}\text{O}_4$ ($x=0.5,0.6$)

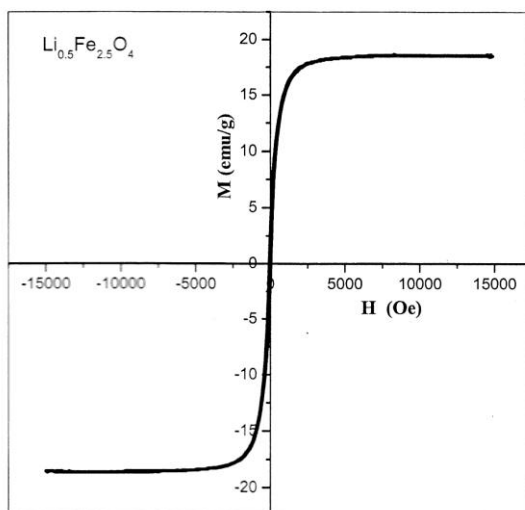


Fig. 1.8.a Hysteresis loops of $\text{Li}_{0.5}\text{Fe}_{2.5}\text{O}_4$

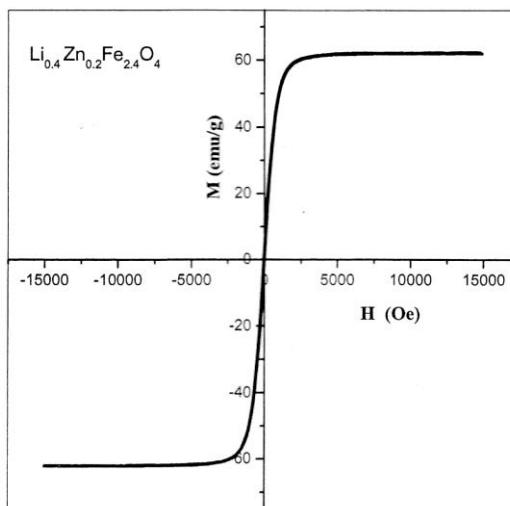


Fig. 1.8.b. Hysteresis loop of $\text{Li}_{0.4}\text{Zn}_{0.2}\text{Fe}_{2.4}\text{O}_4$

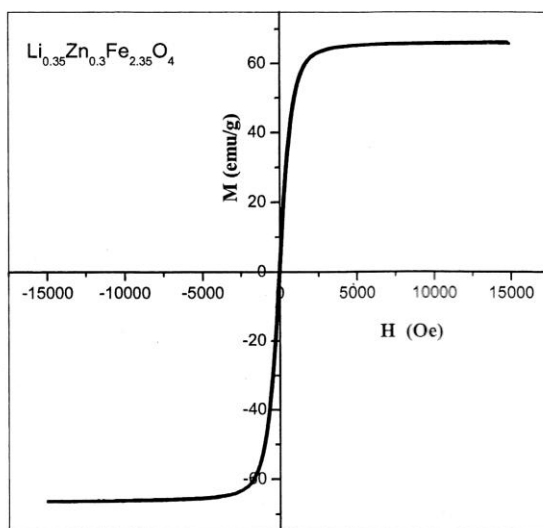


Fig. 1.8.c. Hysteresis loop of $\text{Li}_{0.35}\text{Zn}_{0.3}\text{Fe}_{2.35}\text{O}_4$

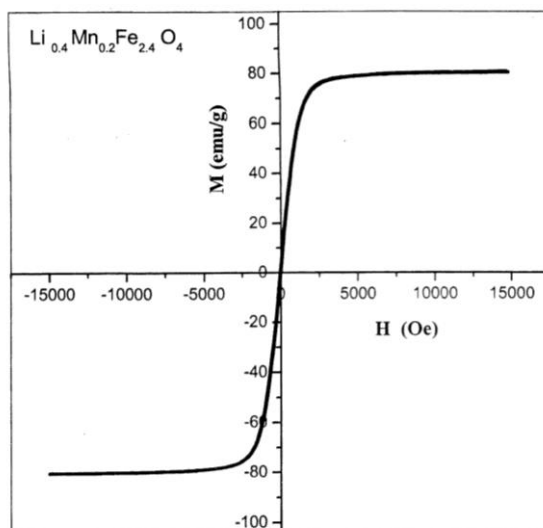


Fig. 1.9.a. Hysteresis loop of $\text{Li}_{0.4}\text{Mn}_{0.2}\text{Fe}_{2.4}\text{O}_4$

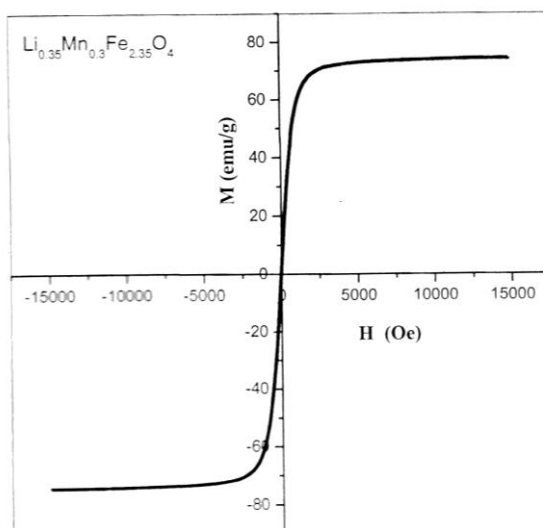


Fig. 1.9.b. Hysteresis loop of $\text{Li}_{0.35}\text{Mn}_{0.3}\text{Fe}_{2.35}\text{O}_4$

From 1.8.a to 1.8.c show the hysteresis loops of LZF samples having composition $x = 0$ to $x = 0.3$ are shown and fig. 1.9.a and 1.9.b shows hysteresis loop of LMF samples having compositions of 0.2 and 0.3.

The magnetization measurements on two ferrite system show by Table 1.5 and 1.6. We can see that LZF samples having $X = 0.3$ has maximum value of saturation magnetization and for LMF samples $x = 0.2$ has maximum value of saturation magnetization.

Zinc substitutions in lithium ferrite are known to cause an increase in the magnetization for low levels of substitution (below $x = 0.3-0.4$) followed by a decrease in magnetization for larger amounts. Mossbauer evidence for a non-collinear spin structure in high $-X$ LiZn ferrite has been found. Large Zn substitutions lead to a non-collinear spin arrangement in Li-Zn ferrites.

The saturation magnetization (M_s) in spinel ferrites are expressed as $M_s = |M_B - M_A|$ with the substitution of Zn^{2+} , the decrease in value of M_A .

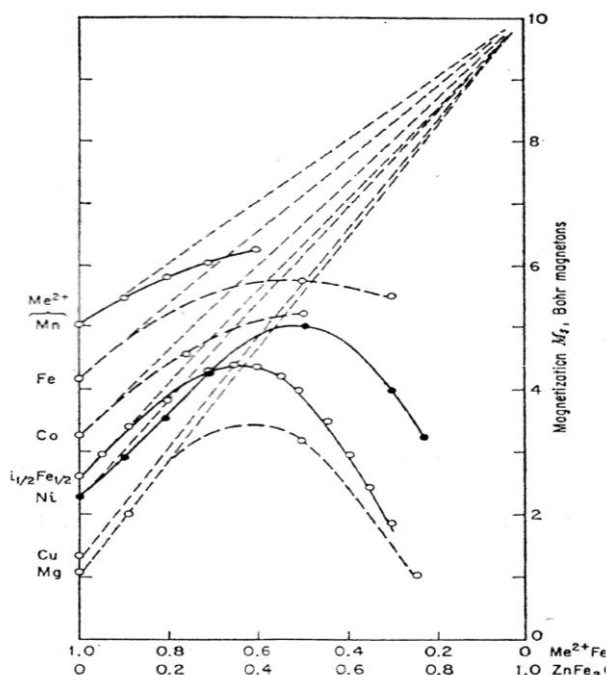


Fig.1.10 Experimental curves of magnetization, in Bohr magnetons per molecule for several zinc substituted ferrites.

In ferrites of the present study zinc has strong preference for A site. Lithium ions populate tetrahedral sites. Initially the Fe³⁺ ions in the B site replaced by lithium and Zn ions. For lithium Manganese ferrites, Manganese has a strong preference for B site. The magnetic ions present in the B sites are Mn²⁺ and Fe³⁺. Hence variations of Mn²⁺ replace the Fe³⁺. This decrease the value of magnetic moment of B site. When x = 0.2, net magnetization increases.

Table (1.5) Magnetization parameters of Lithium Zinc Ferrites at 300K

x	Saturation Magnetization (Ms) emu/gm	Coercivity (Hc) Oe	Remnant Magnetization (Mr) emu/gm
0	18.85	58	2.5
0.2	62.5	26	1.89
0.3	66.5	23	1.9
0.5	50	-	-
0.6	16.67	-	-

Table (1.6) Magnetization parameters of Lithium Manganese Ferrites at 300K

x	Saturation Magnetization (Ms) emu/gm	Coercivity (Hc) Oe	Remnant Magnetization (Mr) emu/gm
0	18.85	58	2.5
0.2	81.3	22	1.65
0.3	74.6	23	2.2
0.5	34.39	-	-
0.6	31.56	-	-

Large substitutions of non-magnetic ions in both A and B sites decrease the magnetization value and the curie temperature.

The variation of coercivity is clear from table 1.2 and 1.3. It is well known that coercivity is dependent on different parameters.

$$\sigma_{M_B} = \frac{\text{Molecular weight} \times \text{saturation Magnetization}}{N \times \mu_B}$$

N is the Avogadro constant, μ_B Bohr magneton

Fig 1.7 shows the variation of σ_{M_B} with Zn and Mn concentration

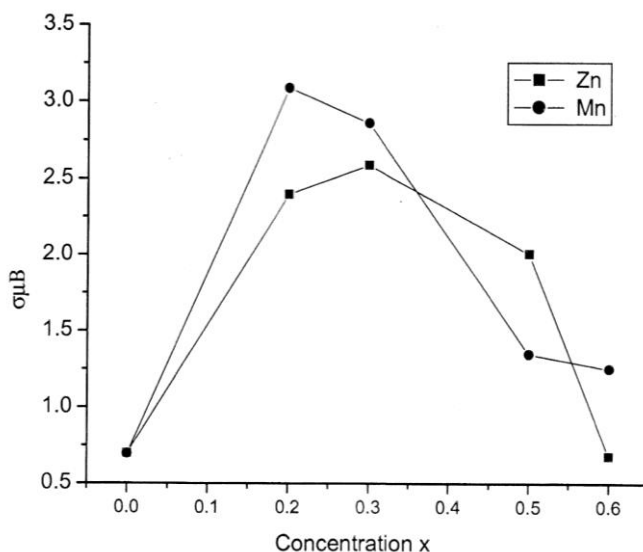


Fig. 1.11 variation of $\sigma\mu_B$ with Zn & Mn concentration

The magnetization increases first with increase in zinc content and reaches a maximum at $x = 0.3$ and then decrease. The A-B interaction weaker due to increase in zinc concentration and this make B-B interaction to dominate. In B site the ionic moments are not parallel to one another. This is called canting of spins and the angles between them determine the moment of the B sublattice. This causes a reduction in B sublattice moments.

The magnetization per formula unit in Bohr magneton for lithium manganese ferrites at first increases and then decreases $\sigma\mu_B$ is maximum for $x = 0.2$.

The variation of magnetic moment with temperature for the samples $\text{Li}_{0.35}\text{Mn}_{0.3}\text{Fe}_{2.35}\text{O}_4$ at 100e and for $\text{Li}_{0.35}\text{Zn}_{0.3}\text{Fe}_{2.35}\text{O}_4$ at 50 e shown in fig. 1.12 & 1.13. The moment increase with increase of temperature.

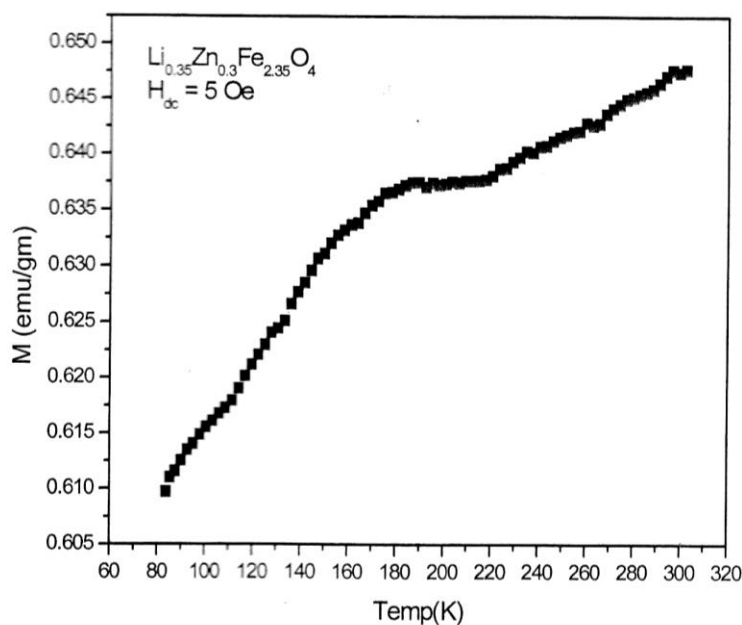


Fig. 1.12 M & T curve of $\text{Li}_{0.35}\text{Zn}_{0.3}\text{Fe}_{2.35}\text{O}_4$

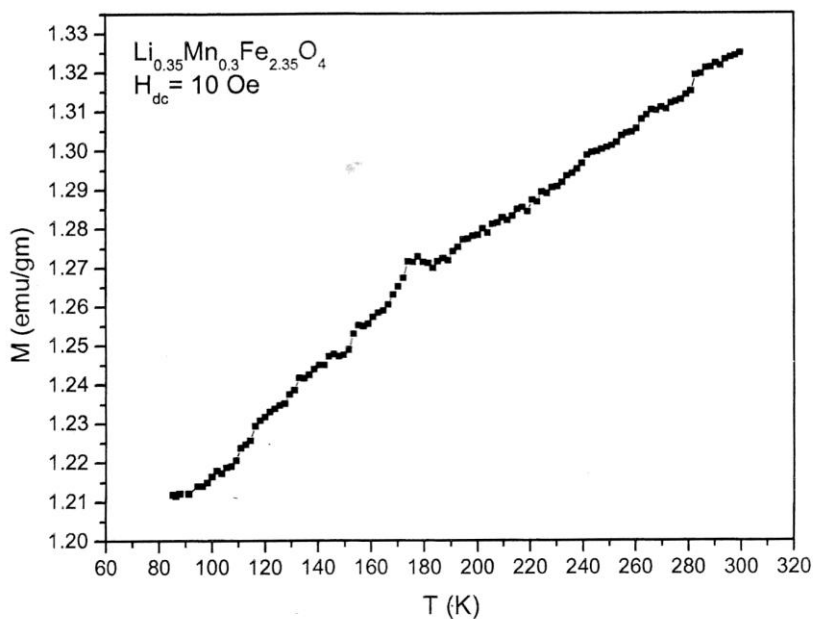


Fig 1.13 M & T curve of Li_{0.35}Mn_{0.3}Fe_{2.35}O₄

The variation between M & H is also measured at 80K for the Zn composition at x = 0.3.

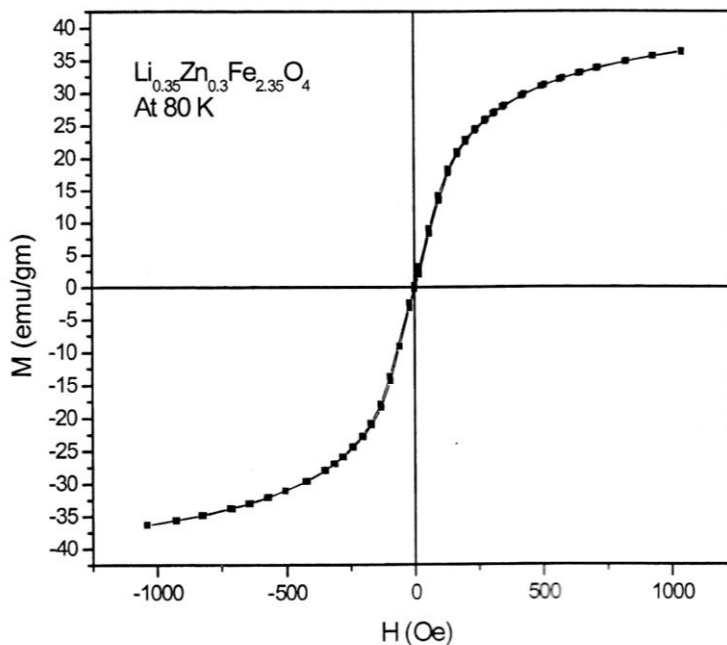


Fig.1.14 Hysteresis loop of Li_{0.35}Zn_{0.3}Fe_{2.35}O₄

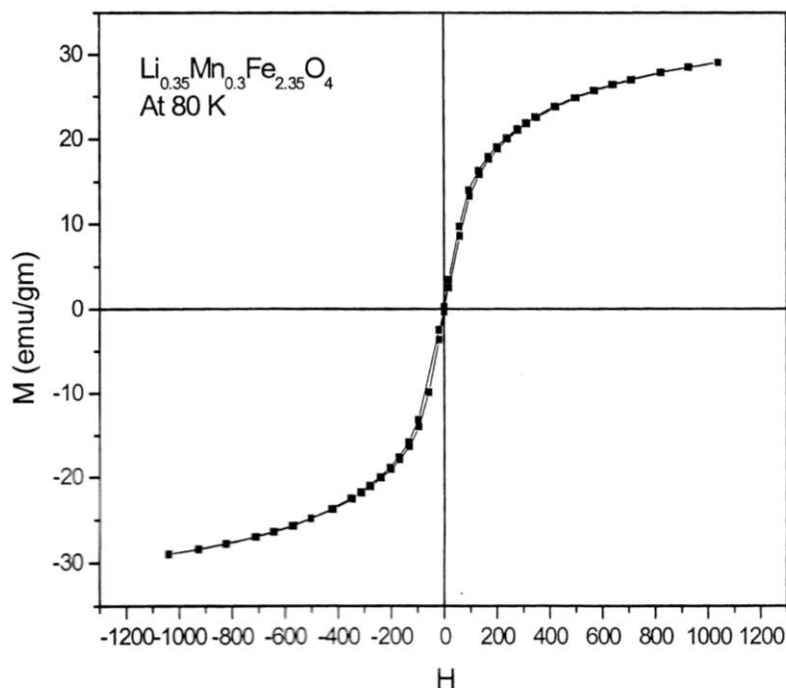


Fig.1.15 Hysteresis loop of $\text{Li}_{0.35}\text{Mn}_{0.3}\text{Fe}_{2.35}\text{O}_4$

Table (1.7) Magnetization parameters at 80K for $x=0.3$

Sample	Saturation Magnetization	Coercivity (Hc) Oe	Remnant Magnetization (Mr) emu/gm
$\text{Li}_{0.35}\text{Zn}_{0.3}\text{Fe}_{2.35}\text{O}_4$	36.275	2.35	0.28
$\text{Li}_{0.35}\text{Mn}_{0.3}\text{Fe}_{2.35}\text{O}_4$	29.2	1.6	0.28

Saturation magnetization for both ferrites is decreased as the temperature is decreased. The coercivity values are also decreased for both the ferrites as the temperature is decreased. Both samples shown same remnant magnetization 0.28 emu/gm at 80K.

1.6 Curie temperature measurements

Curie temperature is measured by Lauria technique. In this arrangement a strong electromagnetic bar inserted in a tubular furnace kept vertically. The sample is attached to the electromagnet. The temperature of the furnace is slowly increased. For a particular temperature, ferrite sample falls freely off from the electromagnet and converted into paramagnetic state. This particular temperature is the curie temperature T_c .

Value, of curie temperature T_c obtained are tabulated in tables 1.8 and 1.9. it is found that T_c for LZF samples decreases linearly and for LMF decreases non linearly with increases of concentrations

The variation of curie temperature with zinc content found to decrease with increase of the zinc level. The curie temperature of the ferrites is determined by the overall strength of AB interaction, but sometimes AA and BB may become important.

Table 1.8 Curie temperature and Zn concentration

Zn composition (x)	Curie Temperature (K)
0.1	>910
0.2	863
0.3	733
0.4	713
0.5	596
0.6	591

The non magnetic Zn ions reduces the density of the magnetic ions in the A-site, thus reducing the net moment of the A sublattice and weakens the AB exchange interaction which is responsible for observed ferrimagnetism.

Table 1.9 Curie temperature and Mn concentration

Mn composition (x)	Curie Temperature (K)
0.2	898
0.3	577
0.4	630
0.5	681
0.6	677

A different behaviour is seen when Mn ions are used. Mn ions decrease the value of M_B , leading to decrease the value of M_S . The effect of Curie temperature is not as pronounced as in the case of substitution by Zn^{2+} . This is because of small decrease in the value of M_B due to Mn^{2+} substitution

1.7 Permeability measurement

One of the most critical magnetic properties of for many ferrite application is the frequency dependence of the complex permeability.

The permeability measurements were carried out on toroidally shaped samples with inner and outer diameter of 0.8 and 1.3cm respectively and thickness of around 2.3 mm. The temperature dependence of the permeability was measured at 1KHz using LCR meter. The temperature was varied from room temperature to 300°C.

Fig. (1.16) shows variation of permeability with temperature for lithium zinc ferrites. The permeability increases with increasing temperature for all ferrite sample. For x=0.5 and 0.6 it forms a small peak just before the Curie temperature and falls beyond the Curie temperature.

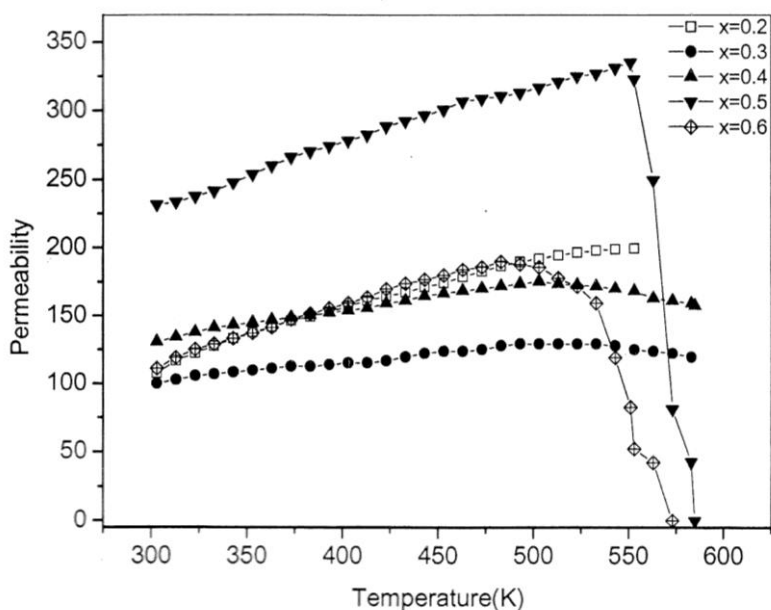


Fig. 1.16 plots of variation of permeability with temperature of lithium zinc ferrites.

Curie temperature measured from Lauria technique and permeability studies for the two concentrations are given in the table 1.10.

Table 1.10 Curie temperature from permeability studies

Zn content x	Lauria method K	Permeability studies K
0.5	596	585
0.6	591	573

Fig. (1.17) shows the permeability Vs temperature curves for lithium manganese ferrite samples from room temperature to 453K.

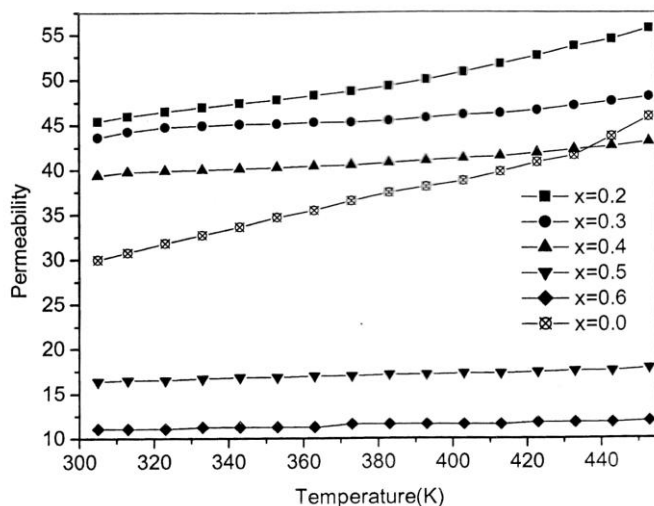


Fig. 1.17 plots of variation of permeability with temperature of lithium manganese ferrites.

The alignment of magnetic moment is disturbed due to thermal agitation and hence the saturation magnetization and anisotropy constant usually decrease with increase of temperature.

1.8 Conclusion

This topic studies the Mossbauer and magnetization properties of Lithium zinc ferrites and Lithium Manganese ferrites. In Lithium zinc Ferrite IS_A is less than IS_B for all samples. The quadrupole splitting dQ_A is greater than dQ_B except for the composition $X = 0.2$. The hyper fine magnetic field at the A and B sites decreases with the increase in the substitution of Zn^{2+} . The replacement of iron atom by zinc as a next nearest neighbours reduces hyperfine field. For Lithium Manganese Ferrites $IS_A < IS_B$ for all the samples. The quadrupole splitting arise from the unbalanced 3d orbital population of Fe ions. The nuclear hyper fine field for A site is lower than that of B-site. In Magnetization measurement, for Zn samples the magnetization reaches the saturation value below a field of 1.5kOe and for the Mn Samples it reaches the saturation values below the field is 2kOe. In curie temperature measurement, T_c for LZf samples decreases linearly and for LMF samples decreases non linearly with increase of concentration. In permeability measurement, for lithium zinc ferrites the permeability increases with increasing temperature for all the ferrite samples. For $x = 0.5$ and 0.6 it forms a small peak just before curie temperature and falls beyond the curie temperature, for lithium manganese ferrite, there is a linear increase of permeability with temperature.

References

- [1]. V. Verma, S.P. Gairola, M.C. Mathpal, S. Annapoorni, R.K. Kotnala, J. Alloys Comp. 481 (2009) 872–876.
- [2]. Bhide, V.G.: Mossbauer Effect and its Applications. Tata McGraw-Hill, New Delhi (1973)
- [3]. Ganser, U. (ed.): Mossbauer Spectroscopy. Springer, New York (1975)
- [4]. M. Srivastava, S. Chaubey, A.K. Ojha, Mater. Chem. Phys. 118 (2009) 174–180. L. Neel, Ann. Phys. (Paris), 3 137 (1948)
- [5]. Hadjipanayis, G.C., Prinz G.A. (ed.): Science and Technology of Nanostructured Magnetic Materials. Plenum, New York (1991)
- [6]. F. Grasset, N. Labhsetwar, D. Li, D.C. Park, N. Saito, H. Haneda, O. Cador, T. Roisnel, S. Mornet, E. Duguet, J. Portier, J. Etourneau, Langmuir 18 (2002) 8209–8216.
- [7]. Sato, T., Haneda, K., Seki, M., Iijima, T.: Morphology and magnetic properties of ultrafine $ZnFe_2O_4$ particles. Appl. Phys. A **50**, 13–16 (1990)
- [8]. C.G. Koops, On the dispersion of resistivity and dielectric constant of some semiconductors at audio frequencies, Physical Review 83 (1951) 121.
- [9]. M.A. Ahmed, N. Okasha, S.I. El-Dek, Nanotech. 19 (2008) 065603.
- [10]. M.A. Iqbal, M. Islam, M.N. Ashiq, I. Ali, A. Iftikhar, H. M. Khan, J. Alloys Comp. 579 (2013) 181–186.
- [11]. M.A. Elhili, J Magn Magn Mater, 136, (1994)
- [12]. Rozman, M., Drogenik, M.: Hydrothermal synthesis of manganese-zinc ferrites. J. Am. Ceram. Soc. **78**, 2449–2455 (1995)
- [13]. R.P. Patil, P.P. Hankare, K.M. Garadkar, R. Sasikala, J. Alloys Comp. 523 (2012) 66–71.
- [14]. E.J.W. Verwey, J.H. De Boer. Cation arrangement in a few oxides with crystal structures of the spinel type, Recueil des Travaux Chimiques des Pays-Bas 55 (1936) 531–540.
- [15]. V.G. Bhide, Mossbauer effect and its Applications, Tata Mc Graw Hill, New Delhi 1973
- [16]. M.A. Dar, K.M. Batoor, V. Verma, W.A. Siddiqui, R.K. Kotnala, J. Alloys Comp. 493 (2010) 553–560.
- [17]. T. Namgyal, J. Singh, K. Chandra, S. Bansal, S. Singhal, J. Mol. Struct. 1019 (2012) 103–109.
- [18]. Alex Goldman, Modern Ferrite Technology, second ed., Springer, New York, 2006.
- [19]. M. Singh, S.P. Sud, Controlling the properties of magnesium– manganese ferrites, Materials Science and Engineering B 83 (2001) 180–184.
- [20]. Roy, M.K., Halder, B., Verma, H.C.: Characteristic length scales of nanosize zinc ferrite. Nanotechnology. **17**, 232–237 (2006)

- [21]. A.K.M.A. Hossain, M.A. Rahman, S.F.U. Farhad, B. Vilquin, H. Tanaka, Phys. B Condens. Matter 406 (2011) 1506–1512.
- [22]. Sumen Sharma & N D Sharma, Ind.J.Pure & Appl. Phys.44, 220-26(2006) Upadhyay, C., Verma, H.C.: Anomalous change in electron density at nuclear sites in nanosize zinc ferrite. Appl. Phys. Lett. **85**, 2074–2076 (2004)
- [23]. Sikander Ali, Alimuddin and V.R Reddy, Pramana, 65, 6, 1121-26(2005)
- [24]. Upadhyay, C., Verma, H.C., Rath, C., Sahoo, K.K., Anand, S., Das, R.P., Mishra, N.C.: Mössbauer studies of nanosize $Mn_{1-x}Zn_xFe_2O_4$. J. Alloys Compd. **326**, 94–97 (2001)
- [25]. J.B. Goodenough, A.L. Loeb, Theory of ionic ordering, crystal distortion, and magnetic exchange due to covalent forces in spinels, Physical Review 98 (1955) 391–408.
- [26]. M. Abdullah Dar, K.M. Batoo, Vivek Verma, W.A. Siddiqui, R.K. Kotnala, Synthesis and characterization of nano-sized pure and Al-doped lithium ferrite having high value of dielectric constant, Journals of Alloys and Compounds 493 (2010) 553–560.
- [27]. P. Ayyub, M. Multani, R. Vijayaraghavan, Phys. Lett. A 119 (1986) 95–99
- [28]. F.W.Oliver, D. Seifu, E.Moffman etal, Applied Py letters, 75, 19, 2993(1999)
- [29]. N.V.Nair, Ph.D Thesis, IIT Kanpur, (1982)
- [30]. K.P. Chae, W.H. Kwon, J.G. Lee, J. Mag. Mag. Mater. 324 (2012) 2701–2705.
- [31]. M. Singh, S.P. Sud, Mg–Mn–Al ferrites for high frequency applica- tions, Modern Physics Letters B 14 (2000) 531–537.
- [32]. Kun Uk Kang, Seong Wook Hyun and Chul Sung Kim, J.Appl. Phys. 99, 08M917 (2006)
- [33]. P. Ayyub, M. Multani, R. Vijayaraghavan, Phys. Lett. A 119 (1986) 95–99.
- [34]. G.K. Shenoy, F.E. Wagner, Mössbauer Isomer Shifts, Amsterdam:North- Holland, 1978.
- [35]. J. Smit, H.P.J. Wijn, Ferrites, Philips Technical Library, Eindhoven (1959).
- [36]. F.Varret, A. Gerard, and P.Imbert, Phys. Status Solidi 43, 723(1971)
- [37]. R.K.Puri, M.Singh, S.P.Sud, Effect of substitution of In $3p$ ions on the electrical and magnetic properties and Mossbauer study of $Mg_{0.9}Mn_{0.1}In_xFe_{2-x}O_4$ ferrites, Journal of Materials Science 29 (1994) 2182–2186.
- [38]. GF.Woude Van der and G.A.Sewatzky, Phy.Rev.B4 3159(1971)
- [39]. H.N. Oak, K.S. Baek, K.S. Yu, J. Phys.: Condens. Matter 10 (1998) 1131–1136. G.O. White, C.E. Patton, J. Magn. Magn. Mater. 9 (1978) 299–317.
- [40]. S. Verma, J. Karande, A. Patidar, P.A. Joy, Mater. Lett. 59 (2005) 2630–2633.
- [41]. S. Verma, P.A. Joy, J. Appl. Phys. 98 (2005) 124312–124320.
- [42]. M. Srivastava, J. Singh, M. Yashpal, D.K. Gupta, R.K. Mishra, S. Tripathi, A.K.Ojha, Carbohydr. Polym. 89 (2012) 821–829.
- [43]. Shalendra Kumar and Alimuddin, J.Appl. Phys.99 08M910(2006)
- [44]. M.De Marco et. al.J.Appl. Phys. 73(10)15(1993)
- [45]. S.Y. An, I.B. Shim, C.S. Kim, J. Mag. Mag. Mater. 290–291 (2005) 1551–1554.
- [46]. M.C.Chhantbar, A.Gismelseed, K.B.Modi, G.J.Baldha, Ali Yousif & H.H.Joshi, Ind J Pure & Appl Phys, 45, 856-859(2007)
- [47]. S.K.Kulshreshtha, J Mater Sci, 5, 638 (1986)
- [48]. Y.P. Fu, S.H. Hu, Ceram. Int. 36 (2010) 1311–1317.
- [49]. G.A.Pettitt & D W. Forester, Phys. Rev. B, 4, 11 (1971)
- [50]. J.J.Van Loef, Physica 32, 2102(1966)
- [51]. G.A. Sawatzky, F.Van Der Woude, and A.H Horrish, Phys. Rev. 187, 747(1969)
- [52]. F.Varret, A.Gerard, and P. Imbert, Phys. Status Solidi 43, 723(1971)
- [53]. R.L.Streever, Phys. Rev. 186, 285(1969)
- [54]. J.Dormann, J.de Phys. C1, 41, 175, (1980)
- [55]. De Lau, J.C.M.Philips Res. Repts. Suppl. (1975) 6, 88-91
- [56]. Sonal Singghal, S K Barthwal & Kailash ChandraInd J Pure & Appl Phys, 45, 821-825(2007)
- [57]. W.H.Kelly, V.J.Folen, M.Hass, W.N.Schreiner and G.B.Beards, Phy.rew, 124, No. 1 (1961)
- [58]. B.J.Evans and S.S. Hafner, J Phys. Chem Solids, 29, 1573 (1968)
- [59]. G.A.Sawatzky, F.Van Der Woude, A.H.Morish, Phys. Rev. 187, 747(1969)
- [60]. B.Viswanathan, V.R.K.Murthy, Ferrite Materials, Science and Technology (Narosa Publishing House) (1990)
- [61]. Smit J and Wijn H P G Ferrites (Philips Techncial Library)(1950)
- [62]. V.C.Wilson and J.S.Kasper, pheps.Rev. 95, 1408 (1954)
- [63]. C.E.Patton, C.A Edmondson and Y.M.Liu, J.Appl. Phys. 53(3)(1982)
- [64]. J.G.Booth, G.Srinivasan, and C.E.Patton, C.M.Srivastava, Solid State Communications, 64 3 287-289(1987)
- [65]. L Neel C.R Acad. Sci. Parid 230, 375(1950)
- [66]. E.W.Gorter, Philips Res. Repts. 9, 295(1954)
- [67]. Y.Yafet and C.Kittel, Phys. Rev. 87, 90(1964)
- [68]. S.Celler, J.Appl. Phys. 37, 1408(1966)
- [69]. N.S.Satyamurthy et al, Phys. Rev. 181, 969 (1966)
- [70]. G.A.Petit and D.W.Forester. Phys. Rev B 4, 3912 (1971)
- [71]. Benjamin Lax, Kenneth J Button, Microwave ferrites and ferrimagnets, Mc Graw-Hill Book Co, (1962)
- [72]. E.W.Gorter., Philips Res Rep. 9, 295 (1954); 9, 403(1954)
- [73]. Jefferson C F and West R J, J.Appl.Phys., 32, 3905(1961)
- [74]. E.W.Gorter, Phil Res., 9a 321(1954)
- [75]. P.B.Baba et al, IEEE Trans. Magn., MAG-8 83 (1972)
- [76]. B.D.Cullity, Magnetic Materials, Addison Weisley Publishing company, Inc (1972)
- [77]. V.C.Wilson and J, S.Kasper, Phys. Rev. 95, 1408(1954)
- [78]. V.I.Goldonski, V.F.Belov, M.N.Devisheva and V.A.Trukhtanov, Sov. Phy. JETP 22, 1149(1966)
- [79]. T.Sato, K.Haneda, N.Seki and T.Iijima, Appl. Phys. A 50, 13-16(1990)
- [80]. Y.Yafet and C.Kittel, Phys Rev 37, 290(1952)
- [81]. J.M.Hastings and L.M. Corliss; Phys. Rev. 102, 1460(1956)
- [82]. M.A.Gilleo, J Phys. Chem. Solids. 13, 33-39(1960)
- [83]. M.A.Gilleo, Phys. Rev. 109, 777(1958)
- [84]. Radhapiyari Laishram, Sumitra Phanjoubam, HNK Sarma and Chandra Prakash Phy.D: Apply. Phys, 32 2151-2154(1999)
- [85]. M.T.Johnson and E.G.Visser, IEE Transaction on Magnetics, Vol 26, No. 5(1990)
- [86]. A Globus, J.De.Phy.38(1977) cl-1 (proc. 3rd Int. Ferrites conf)
- [87]. Mahadev Anapa Madare and Sadanand Vitthal Salvi, Turk J.Phys, 29 25-31(2005)